DOI: 10.1002/cctc.201000403

STEM HAADF Tomography of Molybdenum Disulfide with Mesoporous Structure

Feihong Nan,[a] Chaojie Song,[b] Jiujun Zhang,[b] Rob Hui,[b] Jinwen Chen,[c] Craig Fairbridge,[c] and Gianluigi A. Botton*[a]

A highly ordered mesoporous molybdenum disulfide has been developed for catalysis in heavy oil refining. The morphology, structure, and composition of the material have been systematically characterized with advanced electron microscopy techniques. Scanning transmission electron microscopy with high-angle annular dark field tomography has been used to investigate the porous structure to give spatial information on the nanometre scale, and offer a direct view of individual porous particles in three-dimensions. The pore-size distribution, connectivity of the pores, and the mesoporous surface area have also been analyzed and offer useful information towards catalyst design.

Introduction

Transition metal chalcogenides have been commercially used in the petroleum refining industry to reduce the sulfur and nitrogen content in heavy oil for several decades.[1–3] Owing to accelerated demand and consumption of energy, the availability of easy-to-access conventional light sweet crude oil is declining. The utilization of extra heavy crude oil is becoming more common. However, upgrading and refining heavy oil is more complicated and may emit more greenhouse gases and air contaminants, which result in more environmental concerns than light sweet crude oil. Severe emission restrictions require more environmental friendly fuels with much lower sulfur and nitrogen containing compounds. Therefore, utilization of more effective catalysts than those currently available is one of the most important approaches to meet the new requirements.[4,5] Nanostructured molybdenum disulfide (MoS_2) exhibits a distinct crystal structure with unique physical and chemical properties, and has attracted considerable attention, owing to its high activity in the hydrodesulfurization (HDS) process to produce clean fuel.[6] The controllable nanostructure, particle size, morphology, and/or porosity of unsupported MoS_2 catalysts can increase the number of catalytically active sites, significantly improving the intrinsic HDS catalytic activity.[7] Therefore, the synthesis of nanostructured unsupported MoS_2 has become a promising research direction. As one type of nanostructured materials, mesoporous MoS_2 has been prepared and it has exhibited higher catalytic activity toward hydrodesulfurization.[7] The high surface area, regular porous structure, and unique pore sizes facilitate the diffusion of reactants and decrease the residence time, enhancing its catalytic activity.[8–10]

It is well known that the chemical composition and structure of a catalyst can significantly affect its catalytic activity and performance. Analytical electron microscopy is a well known powerful research tool that can illustrate this information. To investigate the chemical composition and structure of the catalyst and their effect on the activity and performance, advanced electron microscopy methods are required. For example, analytical electron microscopy techniques have been used to directly probe the local information of the catalytically active site at atomic scales.[11,12] Similarly, elemental analysis by using energy dispersive X-ray spectrometry (EDXS) and electron energy loss spectroscopy (EELS) can reveal the composition and distribution of the elements at the sub-nanometre scale.[13–15]

In packed and dense catalyst structures that do not have a periodic 3-dimensional (3D) arrangement, such characterization is an additional challenge as 2-dimensional projections do not fully represent the true structure of the sample. As a result, new techniques providing 3-dimensional morphological information of the sample become essential.[16–19] Over the last decade, 3D-electron tomography has developed and is applied routinely in the study of macromolecules and cells in biology. However, a few challenges have hindered the widespread application and interest of this technique in materials science and engineering. Firstly, unlike typical biological samples with more complex structures, most inorganic materials have been generally well represented by 2D projections. More importantly, the conventional approach used in biology, namely bright-field (BF) tomography, is generally not suitable for crystalline specimens, owing to the non-monotonic intensity of images with orientation and radiation damage of the sample while ex-

[a] F. Nan, Prof. G. A. Botton
Department of Materials Science & Engineering, McMaster University
1280 Main Street West, Hamilton, Ontario,L8S 4M1 (Canada)
Fax: (+1) 905 521 2773
E-mail: gbotton@mcmaster.ca

[b] Dr. C. Song, Dr. J. Zhang, Dr. R. Hui
Institute for Fuel Cell Innovation, National Research Council of Canada
4250 Wesbrook Mall, Vancouver, British Columbia, V6T 1W5 (Canada)

[c] Dr. J. Chen, Dr. C. Fairbridge
CanmetENERGY, Devon, Alberta, T9G1A8 (Canada)

Supporting information for this article is available on the WWW under http://dx.doi.org/10.1002/cctc.201000403.

periments are carried out at high accelerating voltages.[20,21] To improve the performance of the BF tomography in resolving the catalyst structure in three dimensions, electron tomography in low-voltage aberration corrected bright-field has been developed to reduce the effects from nonlinear dynamic diffraction.[17,19] Moreover, in recent years, extensive work has shown that, contrary to BF images, high-angle annular dark-field (HAADF) scanning TEM images, formed by using a scanned focused probe, provide the minimum contrast changes associated with coherent diffraction effect on crystalline samples. In fact, the intensity of STEM HAADF images varies monotonically both with atomic number and specimen thickness, thus making them ideal for the electron tomography reconstruction.[16,18,20]

In the present work, crystalline MoS_2 with highly ordered porous structure was successfully synthesized and characterized by using common physical characterization techniques including X-ray diffraction (XRD) and N_2 adsorption. STEM characterization was performed over the MoS_2 samples by providing direct structural and chemical compositional analysis. In addition, the STEM HAADF tomography technique was applied to MoS_2 to gain relevant information on volume and morphology, and their 3D distribution within the individual particles so as to determine porosity, connectivity and pore-size distribution.

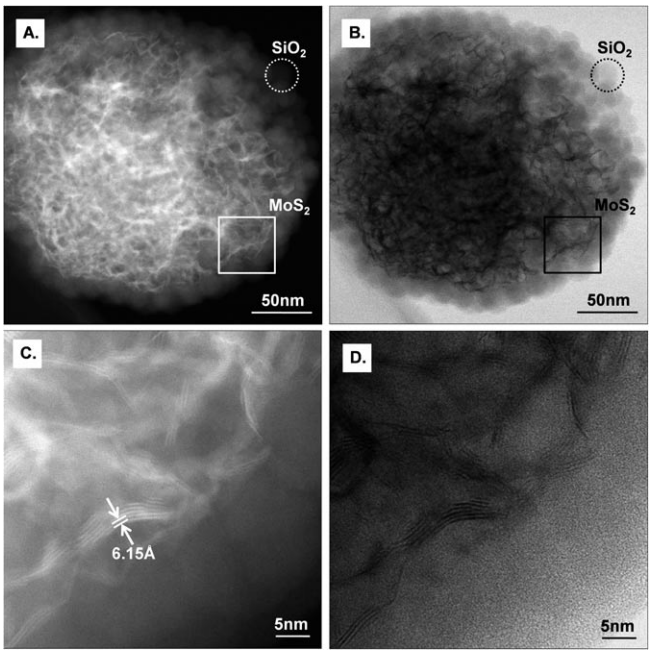

Figure 1. A and B) STEM HAADF and BF images of MoS_2 nanoparticles supported by silica templates at relatively low magnification; C and D) high resolution STEM HAADF and BF micrographs of MoS_2 nanocrystallites distributed inside the interstices of silica template spheres.

Results and Discussion

Physical characterization

The mesoporous material was synthesized by a two-step process whereby the MoS_2 forms within silica nanosphere (22 nm diameter) templates (see further details in the Experimental Section). As a second step, the product is subsequently etched in HF to remove the silica template with a resulting mesoporous MoS_2 structure. The MoS_2 product after HF leaching was characterized by using XRD and N_2 adsorption. XRD patterns showed 4 diffraction peaks at 14.1, 33.6, 40.0, and 59.4° corresponding to the 002, 100, 103, and 110 planes of MoS_2, respectively, in good agreement with the literature.[7] The (002) interplanar distances were found to be 6.23 Å, in close agreement with the value observed in the TEM. Analysis of the N_2 isotherm revealed a BET surface area of 221 m^2g^{-1} with a bimodal porous structure containing pore sizes of 5.8 nm and 18.4 nm, both in the mesopore-size range. The pore size of 5.8 nm was formed from the stacking of the MoS_2 plates on the silica nanospheres, and that of 18.4 nm was from the leaching of the silica template. Template removal might result in shrinking in pore size, forming smaller pores than the template particle size. The pore volume of the material was found to be 0.75 cm^3g^{-1}

HRTEM and EDXS analysis

Following the growth of MoS_2 in the silica template, STEM HAADF (Figure 1A and C) and BF (Figure 1B and D) observations along with the elemental analysis indicate that the templates possess a highly packed structure. MoS_2 crystallites with plane stacking of 4–10 layers are observed. The circular and rectangular areas highlighted in Figure 1A and B correspond to the template sphere and molybdenum disulfide nanocrystallites, respectively. High-resolution images (Figure 1C and D) of the highlighted rectangular area in Figure 1A and B present a layer spacing close to 6.15 Å, which corresponds to the d_{002} of MoS_2, which is consistent with the XRD measurements. Such observations were repeated several times on different particles, giving clear evidence for the presence of MoS_2 nanocrystallites inside the interstices of silica template spheres, which were also confirmed by elemental mapping results (Figure 2).

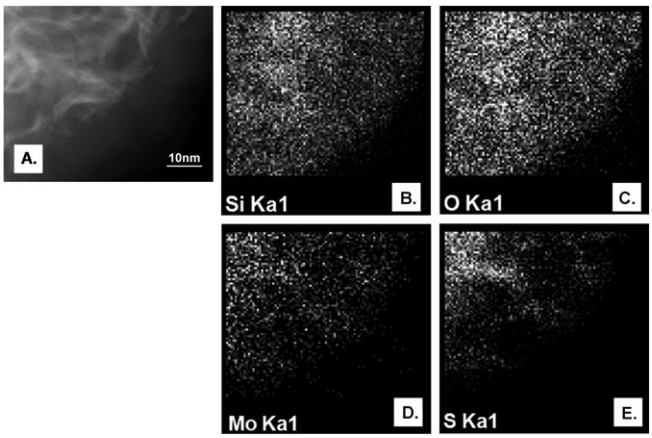

Figure 2. EDXS elemental maps of the MoS_2 grown in the silica templates. A) The STEM image and its corresponding elemental maps of B) Si, C) O, D) Mo, and E) S.

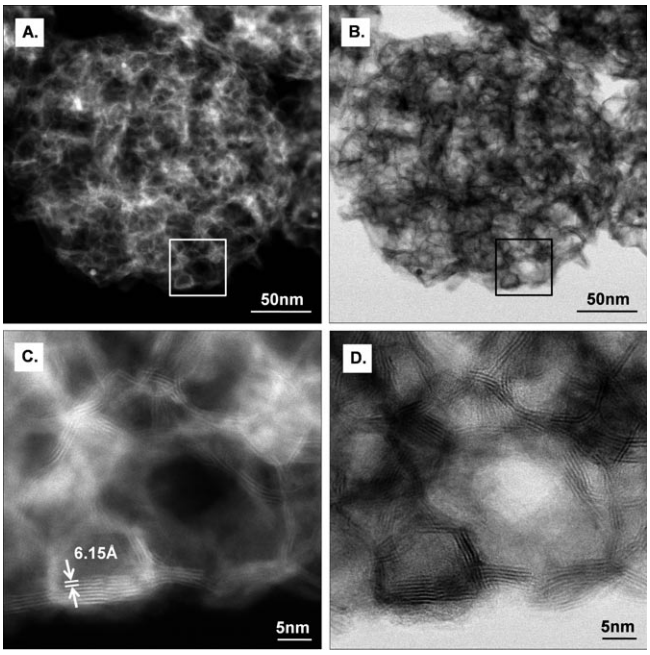

Figure 3. A and B) Overview of the MoS_2 particles at relatively low magnification, after removal of SiO_2 by HF, by using STEM HAADF and bright-field STEM modes, respectively; C) STEM HAADF micrograph of MoS_2 nanoparticles with a highly ordered mesoporous structure; D) detailed view of selected area in BF STEM mode.

STEM observations of the molybdenum disulfide catalysts after the removal of the silica template using HF provide evidence for the presence of a highly dispersed MoS_2 phase with mesoporous structure (Figure 3). The lattice fringes due to the MoS_2 crystallites with 6.15 Å (002) interplanar spacing were clearly observed (Figure 3C and D). Analysis of the elemental mapping (Figure 4) reveals the homogeneous distribution of

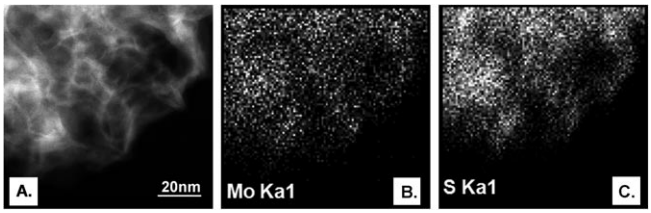

Figure 4. Elemental analysis over MoS_2 after removal of the SiO_2 templates using HF. A) STEM image, and the elemental maps of B) Mo and C) S.

Mo and S. To consider the effect from the overlapping of the S_K and Mo_L EDXS peaks, the $S_{K\alpha}$ and $Mo_{K\alpha}$ lines were selected for the elemental data acquisition and compared. Differences in the S map, as compared to the Mo map, would indicate changes in local Mo/S ratio. EDXS microanalysis performed over several areas revealed that both molybdenum and sulfur were uniformly distributed throughout the sample and that Si, O, and F were not detected (see the Supporting Information).

STEM HAADF tomography

To provide further evidence of the connectivity and the pore-size distribution and to ensure no information could be attributed to the overlapping structures projected in 2D, STEM HAADF tomography was applied to one of MoS_2 particles (diameter of about 500 nm). From the reconstructed volume of the particle (Figure 5) we can observe that the pores inside the

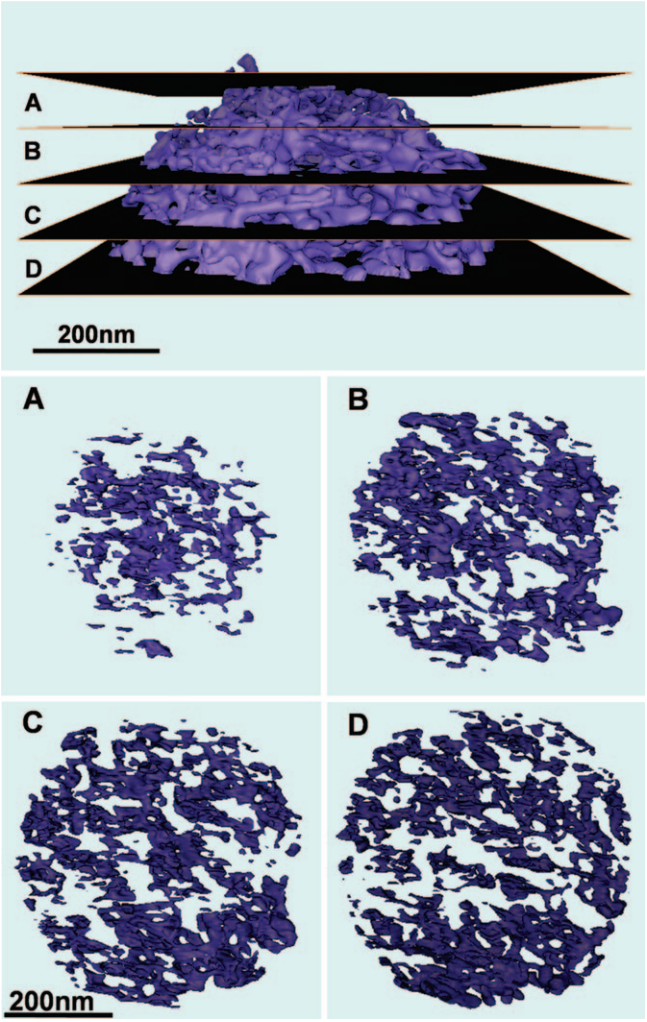

Figure 5. STEM HAADF tomography reconstruction and slice view corresponding to the different locations of a MoS_2 mesoporous particle.

particle are highly interconnected and extend to the surface of the catalyst grain. The size distribution of the pores ranges from 5 nm to 50 nm with a minimal bottleneck diameter of about 5 nm. The opening pores on the particle surface are between 10 nm and 50 nm, thus providing the *meso*-channels to allow heavy crude oil molecules to reach the active sites.[22]

The total surface area (external and internal) of the corresponding particle shown in Figure 1, calculated by counting the voxels of the surface material in contact with the vacuum, was 7.80 μm^2. The volume of the same particle calculated by counting the voxels inside the particle material was 2.46×

10^7 nm^3. From these two measurements based on the tomography reconstruction and the bulk density values of MoS_2, we calculated that a specific surface area of 64.4 m^2g^{-1} for this individual particle. Even though these values are in the same order of magnitude as the value obtained for BET (221 m^2g^{-1}), they are significantly lower. The main origin to this difference is likely related to the contribution of the micropores with sizes smaller than 2 nm, that is, smaller than the resolution of the reconstructed volume, 2.4×2.4×2.4 nm (the size of a single voxel). However, the local tomography measurements are in good agreement with the presence of mesopores of 5.8 nm and 18 nm diameter from N_2 adsorption measurement with the pore-size distribution calculated using the measurement applied to tomography reconstruction volume (Figure 6).

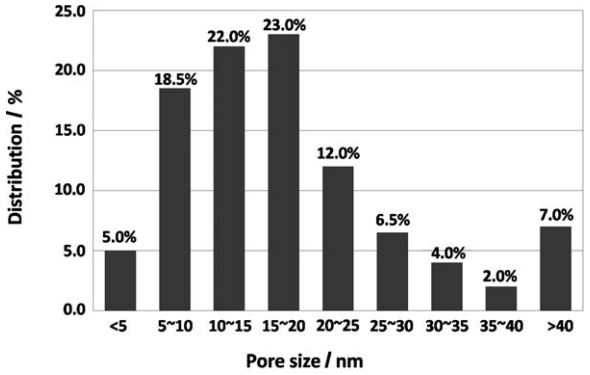

Figure 6. The pore-size distribution of a MoS_2 mesoporous particle.

In addition to the surface area calculation, the distribution of surface area and connectivity of the pores within different regions of the particles can also be calculated (Figure 5). These local measurements from tomography enable the direct visualization of complex structures not possible by other characterization techniques.

Conclusions

STEM HAADF and BF images combined with electron tomography reconstruction have enabled the investigation of molybdenum disulfide catalysts for heavy oil refining. Local measurements of surface area have been performed based on tomographic measurements and have been compared with macroscopic BET data that provides active surface area measurements. The tomography technique also provided information on the structure of the MoS_2 catalyst, in terms of the connectivity of the mesopores, and gave insight into the accessibility of reactant molecules to the inner regions of the particles. Furthermore, the shapes of the pores, the pore volume, and the mesoporous surface area of particles were quantified. Two-dimensional HRTEM characterizations gave evidence of the existence of the mesopores within the crystalline MoS_2. A uniformly distributed mesoporous structure was described according to the elemental analysis by using EDXS.

This information on the pore connectivity provides useful insight into the efficiency and catalytic activity of these materials for cracking of heavy crude oil.

Experimental Section

Synthesis of MoS_2: MoS_2 was synthesized by using ultrasonic spray pyrolysis (USP) according to a literature procedure.[7] First $(NH_4)_2MoS_4$ (2.08 g) was dissolved in deionized water (100 mL), followed by the addition of SiO_2 (6 g, 22 nm) colloid solution. The mixture was then diluted to 200 mL, and stirred for 1 hour. The solution was then loaded into the USP system. The pyrolysis temperature was controlled at 700 °C, and the argon flow rate was 5 L min^{-1}. The product was collected, recovered by filtration, and air dried. The silica template was removed by soaking the product in a 10% HF ethanol solution for 24 h.

Physical characterization of MoS_2: The XRD measurements were performed by using a Bruker D8 X-ray diffractometer equipped with a graphite monochromator and a vertical goniometer with $Cu_{K\alpha}$ radiation. The specific surface area measurement was performed by the BET method in a surface area analyzer (SA3100, Beckman Coulter).

HRTEM imaging and EDX analysis: STEM HAADF and BF imaging were applied to the analysis of molybdenum disulfide samples. Samples for STEM observations were directly supported on a copper mesh with a porous carbon film. Observations in STEM mode were performed by using a FEI Titan 80–300 Cubed transmission electron microscope equipped with a CEOS-designed hexapole-based aberration corrector for the image-forming lens and one for the probe-forming lens and operated at an accelerating voltage of 200 kV. The instrument was also equipped with a Gatan Imaging Filter (GIF) for energy-filtered imaging and an energy dispersive X-ray detector (Oxford Instruments, Inca system) for elemental analysis and mapping.

STEM HAADF tomography: In this work, the tilt series were recorded in the STEM HAADF mode. HAADF-STEM images were acquired by using a FEI Titan 80–300 field emission gun transmission electron microscope operated at 300 kV and with a Fischione high-tilt tomography sample holder. Images were taken with a tilt range from −75 to 70°, and a 2° increment between −50 to 50° and a 1° increment elsewhere. The tilt series without specimen self-shadowing consisted of 95 images. The FEI software package Xplore3D Acquisition was used to control the tilt angle, to maintain the object within the field of view, to correct for focusing, and to record and store 2D images at different tilting angles. Tomographic reconstruction was carried out with the FEI Inspect3D package and visualization as well as the calculation of the reconstructed volume was achieved by using the Amira4.1 package.

Acknowledgements

This work was funded by the Government of Canada's Program for Energy Research and Development, PERD 1.1.3, Petroleum Conversion for Cleaner Air, the Institute for Fuel Cell Innovation, National Research Council Canada, and McMaster University. GAB is grateful to NSERC for funding this project via a strategic grant. Electron microscopy work presented here was carried out at the Canadian Centre for Electron Microscopy, a facility supported by NSERC and McMaster University.

Keywords: EDX spectroscopy · transmission electron microscopy · mesoporous · molybdenum · tomography

[1] R. Nava, J. Morales, G. Alonso, C. Ornelas, B. Pawelec, J. L. G. Fierro, *Appl. Catal. A* **2007**, *321*, 58.
[2] R. Romero-Rivera, A. Del Valle, G. Alonso, E. Flores, F. Castillon, S. Fuentes, J. Cruz-Reyes, *Catal. Today* **2008**, *130*, 354.
[3] T. A. Zepeda, B. Pawelec, A. Olivas, J. L. G. Fierro, *Mater. Res. Innovations* **2007**, *11*, 54.
[4] T. A. Zepeda, B. Pawelec, J. L. G. Fierro, T. Halachev, *Appl. Catal. B* **2007**, *71*, 223.
[5] K. Soni, B. S. Rana, A. K. Sinha, A. Bhaumik, M. Nandi, M. Kumar, G. M. Dhar, *Appl. Catal. B* **2009**, *90*, 55.
[6] S. T. Wang, C. H. An, J. K. Yuan, *Materials* **2010**, *3*, 401.
[7] S. E. S. a. K. S. Suslick, *J. Am. Chem. Soc.* **2005**, *127*, 9990.
[8] Y. F. Shi, Y. Wan, R. L. Liu, B. Tu, D. Y. Zhao, *J. Am. Chem. Soc.* **2007**, *129*, 9522.
[9] Z. D. Huang, W. Bensch, L. Kienle, S. Fuentes, G. Alonso, C. Ornelas, *Catal. Lett.* **2008**, *122*, 57.
[10] Z. D. Huang, W. Bensch, L. Kienle, S. Fuentes, G. Alonso, C. Ornelas, *Catal. Lett.* **2009**, *127*, 132.
[11] P. L. Gai, *Curr. Opin. Solid State Mater. Sci.* **2001**, *5*, 371.
[12] C. Kiely, *Nat. Mater.* **2010**, *9*, 296.
[13] Z. L. Wang, *Adv. Mater.* **2003**, *15*, 1497.
[14] S. Lazar, Y. Shao, L. Gunawan, R. Nechache, A. Pignolet, G. A. Botton, *Microsc. Microanal.* **2010**, *16*, 416.
[15] G. Botton in *Science of Microscopy, Vol. 1* (Ed.: J. C. H. S. Peter W. Hawkes), Springer, **2008**.
[16] J. M. Thomas, P. L. Gal, *Adv. Catal.* **2004**, *48*, 171.
[17] K. P. de Jong, L. C. A. van den Oetelaar, E. T. C. Vogt, S. Eijsbouts, A. J. Koster, H. Friedrich, P. E. de Jongh, *J. Phys. Chem. B* **2006**, *110*, 10209.
[18] I. Arslan, J. C. Walmsley, E. Rytter, E. Bergene, P. A. Midgley, *J. Am. Chem. Soc.* **2008**, *130*, 5716.
[19] M. Bar Sadan, L. Houben, S. G. Wolf, A. Enyashin, G. Seifert, R. Tenne, K. Urban, *Nano Lett.* **2008**, *8*, 891.
[20] M. Weyland, *Top. Catal.* **2002**, *21*, 175.
[21] P. A. Midgley, M. Weyland, T. J. V. Yates, I. Arslan, R. E. Dunin-Borkowski, J. M. Thomas, *J. Microsc.* **2006**, *223*, 185.
[22] O. Ersen, C. Hirlimann, M. Drillon, J. Werckmann, F. Tihay, C. Pham-Huu, C. Crucifix, P. Schultz, *Solid State Sci.* **2007**, *9*, 1088.

Received: November 14, 2010
Published online on March 2, 2011

